Journal of Applied Physics ARTICLE scitation.org/journal/jap

Voltage dependence of equivalent circuit parameters of bilayer organic photovoltaics

Cite as: J. Appl. Phys. **129**, 083104 (2021); doi: 10.1063/5.0035073
Submitted: 25 October 2020 · Accepted: 4 February 2021 ·
Published Online: 23 February 2021

Non Thongprong[1,2,3,a)] and Phillip M. Duxbury[3,a)]

AFFILIATIONS

[1]Nanoscience and Nanotechnology Graduate Program, Office of the Dean, Faculty of Science, King Mongkut's University of Technology Thonburi, Bangkok 10140, Thailand
[2]Theoretical and Computational Science Center (TaCS), Faculty of Science, King Mongkut's University of Technology Thonburi, Bangkok 10140, Thailand
[3]Department of Physics and Astronomy, Michigan State University, East Lansing, Michigan 48824, USA

[a)]**Authors to whom correspondence should be addressed:** non.tho@kmutt.ac.th and Duxbury@pa.msu.edu

ABSTRACT

Despite the very different underlying physics of organic photovoltaics (OPVs), inorganic p-n junction's Shockley's diode equation is often applied to describe current density–voltage (JV) curves of OPVs. The model parameters, including the diode saturation current, diode ideality factor, series, and parallel resistances, are usually extracted and treated as constants in JV curve analyses. In this work, we develop a drift-diffusion bilayer interface (DD-BI) model for bilayer OPVs, which treats the donor–acceptor (D–A) heterojunction using the detailed balance between densities of polaron pairs, free electrons, and free holes. From the DD-BI model, we derive a diode equation, which is of Shockley's equation form, but each parameter is explicitly written in terms of the D–A interface properties. We call this model the self-consistent diode (SCD) model as it is consistent with the DD-BI results provided that the key parameters are from the simulation data. By studying the effects of light intensity and carrier mobility, we find that the Shockley SCD parameters are voltage dependent because of space charge accumulation around the D–A heterojunction. Our models are successful in explaining the common discrepancies in OPV JV curve analyses, such as the validity of fitting for series resistance, deviation of ideality factor from the theoretical values, and different resistance values under light and dark conditions. The results provide a better understanding of OPVs with a D–A heterojunction and how we can capture its physics using the SCD equation.

I. INTRODUCTION

The Shockley equation (SE), which was derived specifically for inorganic p-n junctions,[1] is often applied to describe current density–voltage (JV) curves of organic donor–acceptor (D–A) heterojunction (HJ) solar cells,[2–6] despite fundamental differences between the two systems.[7] Important characteristics of organic D–A HJ solar cells that are different from inorganic cells are lower carrier mobilities[8,9] and lower dielectric permittivity. Lower dielectric constant results in larger exciton binding energy and bound charge-pair states at D–A interfaces, which are usually referred to as charge transfer states or polaron pairs (PPs), while low mobilities enhance the importance of space charge effects.[10] The generalized Shockley equation with parasitic resistances is usually written as

$$J = J_0\left[\exp\left(\frac{q(V_a - JR_s)}{n_{id}k_BT}\right) - 1\right] - J_{ph} + \frac{V_a - JR_s}{R_p}, \quad (1)$$

where J_0 is the diode saturation current density, q is the elementary charge, V_a is the applied or output voltage between the anode and the cathode, R_s is a series resistance, n_{id} is the ideality factor, J_{ph} is a constant photocurrent, and R_p is a parallel resistance.

There are debates among researchers whether the SE can be applied to organic solar cells (OSCs). On the one hand, Wurfel *et al.* disputed the overall applicability of the SE to OSCs on the

grounds that the Shockley parameters, J_0, n_{id}, R_s and R_p, may have no physical meaning in OSCs.[11] On the other hand, equivalent electrical circuit models similar to the SE are successful in describing electrical responses of OSCs in impedance spectroscopy measurements and providing insights into carrier dynamics.[12,13] However, the Shockley parameters are not constants (i.e., they are functions of voltage, light intensity, and charge transport properties[12–14]), so accurate descriptions of the Shockley parameters' behavior are needed.

Giebink *et al.*[15] (GWWF) propose a model for organic D–A HJ equations that are in the same form as the SE, where each parameter is physically meaningful. Liraz *et al.*[16] (LSST) propose an extended interface rate model that includes more processes enabling comparison of different physical effects. However, both of these analytic models require assumptions to estimate implicit quantities, such as the voltage drop across the donor and acceptor regions and the electron and hole densities at the D–A interface (n_I and p_I), which are affected by space charge accumulation in many OPV devices. A more comprehensive approach that treats space charge accumulation more accurately is to use self-consistent drift-diffusion simulations.[17–19] Barker *et al.*[20] developed a drift-diffusion model for organic bilayer solar cells that takes the aforementioned organic properties into account.

Here, we adopt this system of equations to include the interface model of GWWF, and we show a precise connection with Shockley parameters in the self-consistent diode (SCD) model. The SCD equation provides a better understanding of the physical origins of the Shockley parameters including their dependence on applied voltage; and thus, answers questions about the validity of using the Shockley equation to describe JV curves of organic bilayer PV devices. In principle and qualitatively, we can apply this understanding to other photovoltaics with similar layer structures, such as interdiffusion bilayer OPV[21] and organic salt photovoltaics.[22,23]

This paper focuses on introducing the SCD and DD-BI models, and showing how the voltage dependence of the SCD parameters reflect the fundamental physics of device models. We arrange the paper as follows. Section II is a theory section with two parts. The first part introduces the SCD equation and gives the relations of the SCD parameters to the quasi-Fermi energies for holes and electrons. The second part outlines the DD-BI device model and shows how the electron and hole quasi-Fermi energies are calculated from DD-BI calculations. Section III of the paper shows the voltage dependence of the equivalent circuit (SCD) parameters for a typical poly (3-hexylthiophene-2,5-diyl)/phenyl-C61-butyric acid methyl ester (P3HT/PCBM) bilayer device. Note that interdiffusion heterojunctions with a donor-rich region near the anode and an acceptor-rich region near the cathode usually develop in this system even when using a sequential layer deposition method using orthogonal solvents.[21,24,25] However, instead of using the bulk heterojunction drift-diffusion model[17] which considers the blend of donor and acceptor molecules as a single active layer, we consider a donor–acceptor (D–A) heterojunction analogous to that of the inorganic p-n junction so we can gain physical insights into the diode properties of the D–A heterojunction in terms of D–A interface properties.

In the results section (Sec. III), we start from the effects of light intensity and voltage on the key D–A interface parameters. We then vary hole mobility to study the effects of space charge accumulation on the SCD parameters through the changes of carrier densities and quasi-Fermi levels. We explain why a constant resistance value is not sufficient to describe the diode characteristic. The correlations between series, parallel, and total solar cell resistances are explained later in the section. Section IV contains a discussion and summary of the key results of the paper. The supplementary material contains details of the implementation of the DD-BI model and some additional computational results that may be of interest to some readers.

In closing this introductory section, it is important to note that extensions of the GWWF model, such as the LSST model, and the inclusion of new physical effects are required for quantitative comparison with selected experimental systems over the full voltage range. However, the main purpose of this paper is to demonstrate precise relations between an important device model for bilayer OPVs and the self-consistent Shockley Diode equation. This analysis indicates that diode models of OPV IV response are consistent with bilayer OPV device simulations provided the Shockley parameters are voltage dependent. In the conclusion section, we argue that this voltage dependence is quite generic and persists in OPV device models that include a variety of additional physical effects. An important improvement of the DD-BI model used in the main text is to use a SRH recombination expression instead of the reduced form used in GWWF. In the supplementary material, we show that the voltage dependence of the Shockley parameters found in the simple recombination expression used by GWWF persists for a wide range of SRH model parameters, though with quantitative changes for some parameter values.

II. THEORY

Figure 1 summarizes the modified GWWF interface model that is the basis for the DD-BI model and the SCD equation. Devices in this study consist of an anode, a donor layer, the D–A interface with a width a_0, an acceptor layer, and a cathode. We model the interface as a thin layer of mixed donor and acceptor molecules, having the energy levels at the highest occupied molecular orbital edge (E_{HOMO}) and the lowest unoccupied molecular orbital edge (E_{LUMO}) equal to E_{HOMO} of the donor and E_{LUMO} of the acceptor, respectively. As a result of photoexcitation, donor excitons diffuse to the interface with a current density J_X. Then, excited electrons transfer to acceptor molecules, forming interface polaron pairs (PPs) or charge transfer excitons.[10,26–28] The rate at which PPs reach the interface is J_X/a_0. Dissociations of PPs lead to free interface electrons and holes with densities n_I and p_I, respectively, at a rate of $k_{PPd}\zeta$, where k_{PPd} is PP dissociation coefficient and ζ is PP density. PPs can also recombine to ground states at a rate of $k_{PPr}\zeta$, where k_{PPr} is PP recombination coefficient. PPs also come from recombination between interface free carriers (R) and thermal excitations of ground-state electrons (ζ_{eq}). Thermal equilibrium conditions, which are denoted by eq, are when $J_X = 0$ and $V_a = 0$. R is general, and in the detailed calculations described in Sec. III, trap-assisted recombination is used for organic photovoltaic (OPV) examples. Summing all processes involving n_I and p_I

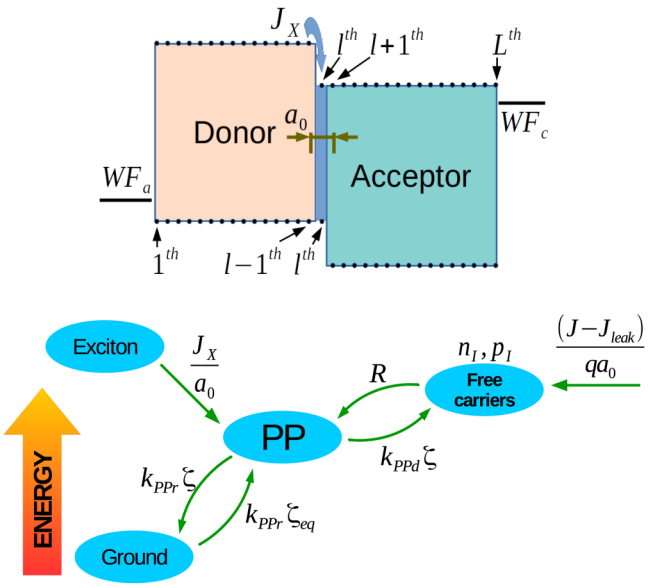

FIG. 1. (Upper figure) An energy level diagram showing the device structure in this study. The dots represent the discretized spatial variable (x) or mesh points used in the DD-BI model. There are L mesh points, and the mesh separation length (δx) between points is constant. We assume all processes involving PPs and interface free carriers (described in the lower figure) occur in the D–A interface region at the lth mesh point. (Lower figure) A diagram summarizing important rates at the D–A interface that affect interface PP density (ζ) and interface free carrier number densities (n_I and p_I). Adapted from Ref. 15.

yields the total current density J. Note that we include a local leakage current density (J_{leak}) to J, which we use to describe leakage current in the dark.

A. The self-consistent diode (SCD) equation

The SCD equation is an analytical expression for OPV JV characteristics that is in the same form as the Shockley equation. It can accurately reproduce results from the drift-diffusion DD-BI device model, provided the SCD parameters are correctly extracted from the DD-BI model results. The SCD equation is an extension of the GWWF model,[15] which expresses the diode voltage and Shockley parameters in terms of quasi-Fermi energies and to include a leakage current in the dark.

Applying the detailed balance principle to ζ, n_I, and p_I, which are in steady states during solar cell operation, we obtain two interface rate equations,

$$\frac{J_X}{a_0} - k_{PPr}(\zeta - \zeta_{eq}) - k_{PPd}\zeta + R = 0, \tag{2a}$$

$$k_{PPd}\zeta - R + \frac{(J - J_{leak})}{qa_0} = 0. \tag{2b}$$

Solving Eq. (2) yields an expression for the current J as

$$J = qa_0(1 - \eta_{PPd})R_{eq}\left(\frac{R}{R_{eq}} - \frac{k_{PPd}}{k_{PPd,eq}}\right) - qJ_X\eta_{PPd} + J_{leak}, \tag{3}$$

where η_{PPd} is the PP dissociation probability expressed by $\eta_{PPd} = k_{PPd}/(k_{PPd} + k_{PPr})$,[29,30] R_{eq} and $k_{PPd,eq}$ are free carrier recombination rate and PP dissociation coefficient at equilibrium, and $-qJ_X\eta_{PPd}$ is the voltage-dependent photocurrent.

The recombination rate R depends on the interface densities n_I and p_I. Generally, under illumination or bias, electrons and holes relax to achieve quasi-thermal equilibrium,[31] where Fermi-Dirac statistics with separate quasi-Fermi energies (E_{fn} for electrons and E_{fp} for holes) can describe n and p,

$$n = N_{LUMO}\exp\left[\frac{-(E_{LUMO} - E_{fn})}{k_BT}\right], \tag{4a}$$

$$p = N_{HOMO}\exp\left[\frac{-(E_{fp} - E_{HOMO})}{k_BT}\right]. \tag{4b}$$

As a result, R usually contains an exponential function of E_{fn} and E_{fp} and a pre-factor term, which can be written in a general form as[32]

$$R = R_{eq}\exp\left(\frac{\Delta E_{fI}}{n_{id}k_BT}\right), \tag{5}$$

where

$$\Delta E_{fI} = E_{fn,I} - E_{fp,I} \tag{6}$$

is the difference in quasi-Fermi energies at the OPV interface.

We find that this form of R provides consistent numerical values of n_{id} with theories. For example, in the case of bimolecular recombination,[33,34] $R = \beta n_I p_I$, where β is a recombination coefficient. We obtain from Eq. (4) that

$$R = \beta N_{LUMO}N_{HOMO}\exp\left(\frac{-\Delta E_{HL}}{k_BT}\right)\exp\left(\frac{\Delta E_{fI}}{k_BT}\right), \tag{7}$$

where ΔE_{HL} is the interface energy gap equal to acceptor E_{LUMO} minus donor E_{HOMO}. At equilibrium conditions where the quasi-Fermi levels do not split from the intrinsic Fermi level (E_f), i.e., $\Delta E_{fI} = 0$, we have

$$R_{eq} = \beta N_{LUMO}N_{HOMO}\exp(-\Delta E_{HL}/k_BT), \tag{8}$$

and hence Eq. (7) is in the same form as Eq. (5) with $n_{id} = 1$ as it must.

Substituting Eq. (5) for R in Eq. (3) yields our proposed general ideal diode equation for organic D–A PV with arbitrary

recombination processes,

$$J = qa_0(1-\eta_{PPd})R_{eq}\left(\exp\left(\frac{\Delta E_{fl}}{n_{id}k_BT}\right)-\frac{k_{PPd}}{k_{PPd,eq}}\right) - qJ_X\eta_{PPd} + J_{leak}. \tag{9}$$

With $k_{PPd}/k_{PPd,eq} \approx 1$ as suggested by GWWF,[15] Eq. (9) is of a form similar to the Shockley form in Eq. (1), and it defines the diode saturation current as

$$J_0 = qa_0(1-\eta_{PPd})R_{eq}. \tag{10}$$

In order to make contact with device models, we need to relate the various terms in Eq. (9) to Eq. (1) by relating the equivalent circuit parameters to the quasi-Fermi energies and other quantities in the device models. These relations are as follows.

1. Series resistance

According to Eqs. (1) and (9), the voltage across the Shockley diode, or photovoltaic voltage, is given by[35]

$$V_d = V_a - J(V_a)R_s = \frac{\Delta E_{fl}}{q}, \tag{11}$$

which is the difference in quasi-Fermi energies in the middle of the interface region.

An obvious but important consequence of the equation is that the voltage at the D–A interface differs from the voltage across the electrodes (V_a) by JR_s. Hence, we have the definition of the voltage-dependent series resistance, $R_s(V_a)$, as

$$R_s(V_a) = \frac{V_a - \Delta E_{fl}/q}{J(V_a)}. \tag{12}$$

The argument V_a will be dropped for simplicity. Because, V_a is the difference between anode and cathode Fermi energies (WF_a and WF_c) under bias,

$$qV_a = WF_c(V_a) - WF_a(V_a). \tag{13}$$

Equation (12) defines R_s as the sum of the change of electron quasi-Fermi energy, in electronvolt, from the cathode to the interface plus the change in the hole quasi-Fermi energy from the anode to the interface, divided by the current density. In devices with multiple layers, changes of E_{fn} and E_{fp} arise from bulk transport and contact resistance[12,36] and can occur in any layers and interfaces so that the expression generalizes by taking a sum of all of the changes in quasi-Fermi energy. In this way, layers and contacts between layers can each be represented by its own value of R_s.

The definition of R_s in Eq. (12) is valid even at open-circuit conditions where $J = 0$ because quasi-Fermi levels align from the D–A interface to the electrodes, i.e., $V_{oc} = \Delta E_{fl}|_{V_a=V_{oc}}$,[37,38] and, thus, both the numerator and the denominator approaches zero, making $\lim_{V_a\to V_{oc}} R_s$ finite and solvable using L'Hospital's Rule.

2. Ideality factor

According to Eq. (5), a general expression for n_{id} with arbitrary recombination types R is

$$n_{id} = \frac{\Delta E_{fl}}{k_BTln(R/R_{eq})}. \tag{14}$$

Hence, n_{id} measures the change in recombination rate ratio $ln(R/R_{eq})$ at any V_a compared to the interface quasi-Fermi level splitting. We also note that Eq. (14) reduces to the expression proposed by Foertig *et al.*[5] [see e.g., Eq. (11) of their paper] at open-circuit voltage where $\Delta E_{fl} = V_{oc}$, which is derived differently.

3. Parallel resistances

One of the simplest ways to extract parallel resistance (R_p) from a JV curve is to use $R_p = [\partial J/\partial V_a]^{-1}_{V_a=0}$,[39] i.e., R_p governs the slope of a JV curve at $V_a = 0$ where higher slopes correspond to lower R_p values. However, R_p values measured under dark and illumination conditions usually differ by orders of magnitude.[40] Based on our simulations, which will be shown further in Sec. III E, the difference comes from the fact that leakage mechanisms under illumination are distinct from those in the dark.

By writing the voltage-dependent photocurrent term $-qJ_X\eta_{PPd}$ as $-qJ_X + qJ_X(1-\eta_{PPd})$, the first term is the constant exciton current supplying the interface, and the second current is due to the total loss of excitons to ground states via PP recombination (i.e., $1-\eta_{PPd}$). The latter accounts for a finite slope of a light JV curve at $V_a = 0$ and can be considered as a leakage current. Let R_{p_PP} be a recombination resistance of PP states that controls this leakage current $qJ_X(1-\eta_{PPd})$. We can write R_{p_PP} from Eqs. (1) and (11) as

$$R_{p\_PP} = \frac{\Delta E_{fl}}{q^2J_X(1-\eta_{PPd})}. \tag{15}$$

The local leakage current (J_{leak}) is another leakage current in Eq. (9), which is necessary for device simulations in the dark (see Sec. III E). The actual mechanism behind the local leakage current is not fully understood, but trap-assisted tunneling processes[41,42] are sometimes important. For simplicity, we model J_{leak} similarly to the leakage current in Eq. (15) as

$$R_{p\_local} = \frac{\Delta E_{fl}}{qJ_{leak}}, \tag{16}$$

where R_{p_local} is a fitting parameter.

Another process that causes a linear response of photocurrent at short-circuit conditions is photoconductivity.[43,44] We did not include this process because the device we used to validate our model with the optimal active layer thickness[45] shows high FF values and with no apparent linear slope of JV curves at short-circuit conditions. However, our model for J_{leak} in Eq. (16), which reads $J_{leak} = R^{-1}_{p,local}\Delta E_{fl}/q$, is in the same form as the photoconductivity current (J_{pc}) model in the work by Renshaw *et al.*,[43] i.e., $J_{pc} = S_{pc}(V_a - JR_s - V_{bi})$, where S_{pc} is the effective photoconductance (reciprocal of resistance). Our $R_{p,local}$ value of $2000\Omega m^2$ (see

Sec. III E) is consistent with their S_{pc} at zero illumination intensity ($S_{pc,0}$) within an order of magnitude.

In the presence of light, both the recombination current $qJ_X(1-\eta_{PPd})$ and the local leakage current J_{leak} occur, which can be modeled by two parallel resistances (R_{p_PP} and R_{p_local})[46] (see Fig. 2). Accordingly, the total parallel resistance under illumination is

$$R_{p,\text{illumination}} = \left(\frac{1}{R_{p\_PP}} + \frac{1}{R_{p\_local}}\right)^{-1}. \tag{17}$$

In most devices, the leakage current $qJ_X(1-\eta_{PPd})$ is much larger than J_{leak} (i.e., $R_{p\_PP} \ll R_{p\_local}$), so $R_{p,\text{illumination}} \approx R_{p\_PP}$.

In the absence of light, the leakage current $qJ_X(1-\eta_{PPd})$ vanishes, leaving J_{leak} as the only leakage pathway. Hence, total R_p in the dark is given by

$$R_{p,\text{dark}} = R_{p\_local}. \tag{18}$$

The difference between $R_{p,\text{illumination}} \approx R_{p\_PP}$ and $R_{p,\text{dark}} \approx R_{p\_local}$ leads to the discrepancy of measured R_p values under different conditions,[11,40] which will be discussed further in Sec. III E.

4. The SCD equation and its equivalent electrical circuit model

Putting together the results from above, we arrive at the SCD equation, which is a general JV relation in the Shockley equation form that can incorporate any recombination type,

$$J = J_0\left[\exp\left(\frac{q(V_a - JR_s)}{n_{id}k_BT}\right) - 1\right] - qJ_X + (V_a - JR_s)\left(\frac{1}{R_{p\_PP}} + \frac{1}{R_{p\_local}}\right), \tag{19}$$

where the equivalent circuit parameters J_0, R_s, n_{id}, R_{p_PP}, and R_{p_local} are defined in Eqs. (10), (12), (14), (15), and (16), respectively.

The equivalent electrical circuit (EEC) model corresponding to the SCD equation is given in Fig. 2, where each electrical component directly represents a real physical process in a bilayer OPV system. Thus, a single diode model where the EEC parameters are allowed to be voltage dependent gives a faithful representation of the true device physics. We now illustrate this correspondence and the typical dependence of EEC parameters on applied voltage by using device model calculations.

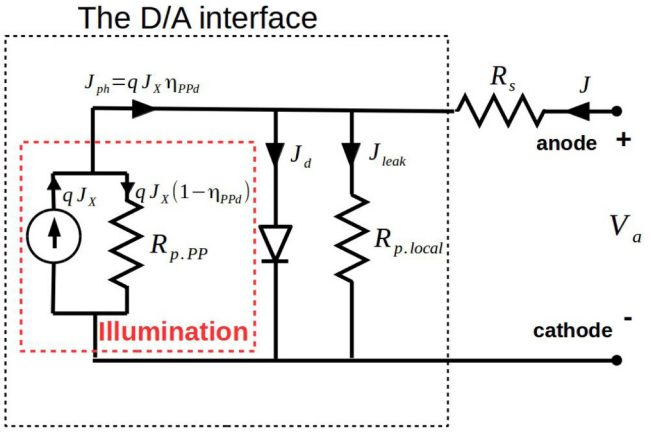

FIG. 2. An equivalent electrical circuit (EEC) model of the SCD equation [Eq. (19)] that has the total current (J) composed of the following component currents: the diode current J_d; the total photocurrent $J_{ph} = qJ_X\eta_{PPd}$; and the local leakage current J_{leak}.

B. The drift-diffusion for bilayer interface (DD-BI) model

The DD-BI model is a one-dimensional drift-diffusion model that implements the modified GWWF interface model in Fig. 1. The model solves the Poisson equation, current continuity equations, and drift-diffusion equations self-consistently as follows. The Poisson equation is given by

$$\frac{\partial^2}{\partial x^2}\psi = \frac{q}{\epsilon}[n + n_t - p - p_t], \tag{20}$$

where ψ is the electrostatic potential; n and p are free electron and hole concentrations, respectively; n_t and p_t are trapped electron and hole densities, respectively; and ϵ is the permittivity. The current continuity equations are given by

$$\begin{aligned}\frac{\partial}{\partial x}J_n &= qU,\\ \frac{\partial}{\partial x}J_p &= -qU,\end{aligned} \tag{21}$$

and the drift-diffusion constitutive equations are given by

$$\begin{aligned}J_n &= -qn\mu_n\frac{\partial}{\partial x}\psi + q\mu_n V_t\frac{\partial}{\partial x}n,\\ J_p &= -qp\mu_p\frac{\partial}{\partial x}\psi - q\mu_p V_t\frac{\partial}{\partial x}p.\end{aligned} \tag{22}$$

Here, $J_{n(p)}$ is the electron (hole) current density, U is the total free carrier generation rate equal to $k_{PPd}\zeta - R$ (see Fig. 1), $\mu_{n(p)}$ is the electron(hole) mobility, and $V_t = k_bT/q$ is the thermal voltage. Here, we use the Einstein relation for the diffusion constant.[47] We neglect carrier generation in the bulk donor and acceptor layers because free carriers cannot be photo-generated from excitons without the D–A interface. Bulk carrier recombination is not included because electrons (holes) are the only majority carriers in

the acceptor (donor) [see the carrier densities in Fig. 6(a)]. We use Boltzmann statistics for free carriers' boundary conditions (see the supplementary material). Note that in order to include electrode's Fermi level pinning effects that cause induced bandgap narrowing and minority carrier recombination near the electrodes, image charge potential at the metal contact should be included as suggested by Magen and Tessler.[48] However, as also suggested in the work,[48] there are negligible minority carriers near the electrodes in the bilayer structure, so the effects are not detrimental.

The variables ψ, n, n_t, p, p_t, J_n, andJ_p depend on position x from the anode and are the key outputs from solving the above equations. The total current density J is the summation of J_n and J_p.

Solving Eqs. (20)–(22) numerically requires discretizations of all the variables into discrete values at mesh points as shown in Fig. 1. We use a constant mesh separation width (δx) of 1 nm, and the 1st and the Lth mesh points are donor and acceptor regions adjacent to the anode and the cathode, respectively. We assume the D–A interface is 1-nm thick from the $l-1$th to $l+1$th nodes, so the lth node, which is in the middle of the D–A interface, is the only node where carrier recombination and generation takes place.

We use an implicit Scharfetter–Gummel method[49] to solve the equations above, as has proven successful for bulk heterostructure devices;[17] however, the bilayer device model is more difficult to converge due to the sharp change in charge densities at the interface. Details of the computational methods are given in the supplementary material.

To make the connection to the interface model in Fig. 1, we calculate the electric field at the interface (F_I), the PP density, and the rates k_{PPd} and k_{PPr}. The electric field F_I is positive when it points from the acceptor to the donor, i.e., the field promotes dissociation. In this case, the dissociation rate, k_{PPd}, is described by the Onsager–Bruan model,[29] which is given by

$$k_{PPd} = \frac{3}{4\pi a_0^3} k_{rec} \exp(-E_b/k_B T) \frac{J_1[2\sqrt{-2b}]}{\sqrt{-2b}}, \tag{23}$$

where $k_{rec} = q(\mu_n + \mu_p)/\epsilon$ is the Langevin bimolecular recombination coefficient, $E_b = q^2/(4\pi\epsilon a_0)$ is the PP binding energy, J_1 is the first order of Bessel function of the first kind, and $b = q^3 F_I/(8\pi\epsilon k_B^2 T^2)$. If F_I is pointing from the donor to the acceptor, so the field aids recombination, the calculation procedure as suggested by GWWF is used, i.e., an additional barrier equal to $-qF_I r_c cos\theta$, where $r_c = q^2/(4\pi\epsilon k_B T)$ is the Onsager radius and θ is the angle between PP separation length vector and D–A interface normal vector is added to the PP binding energy instead of using the Bessel function. k_{PPd} is averaged over the half-sphere using the following expression:

$$k_{PPd} = \frac{1}{\pi} \int_{-\pi/2}^{\pi/2} \frac{3}{4\pi a_0^3} k_{rec} \exp\left[\frac{-E_b + qF_I r_c \cos\theta}{k_B T}\right] d\theta. \tag{24}$$

The PP recombination rate is described by

$$k_{PPr} = k_{PPr,0} \exp\left(\frac{-qF_I a_0}{k_B T}\right), \tag{25}$$

where $k_{PPr,0}$ is the zero-field recombination rate.[50] Note that the sign of F_I is inverted from that of Ref. 50, so the definition of F_I is consistent with the k_{PPd} equations. The interface PP density is given by [Eq. (2)]

$$\zeta = \frac{J_X/a_0 + k_{PPr}\zeta_{eq} + R}{k_{PPr} + k_{PPd}}. \tag{26}$$

Here, we use the recombination rate (R) for trap-assisted recombination in the same form as in GWWF,

$$R = \frac{q\mu_n}{\epsilon} n_I p_{It} + \frac{q\mu_p}{\epsilon} p_I n_{It}. \tag{27}$$

Each term in Eq. (27) is a reduced Shockley–Read–Hall (SRH) recombination[51,52] via donor HOMO tail states and acceptor LUMO tail states in the limit that the hole capture rate is much higher than electron capture rate in the donor and *vice versa* for the acceptor, so the SRH recombination can be considered as bimolecular recombination between localized trapped charges and mobile free carriers.[53–55] See Sec. SII in the supplementary material for the validity of using Eq. (27) to approximate the full SRH form including thermal emission from trap states.

We calculate trapped carrier densities in Eq. (27) using exponential trap distributions.[56,57] Acceptor trapped electron density at the interface (n_{It}) is approximated by the relation,[15]

$$\begin{aligned} n_{It} &\approx H_A exp\left(\frac{E_{fn,I} - E_{LUMO,I}}{k_B T_{t,A}}\right), \\ n_{It} &\approx H_A \left(\frac{n_I}{N_{LUMO}}\right)^{\frac{T}{T_{t,A}}}, \end{aligned} \tag{28}$$

where $k_B T_{t,A} = E_{t,A}$ is the width of acceptor tail states and H_A is the total trap density at the acceptor LUMO band edge. A similar expression can be written for interface donor trapped hole density (p_{It}) having the energetic width of $E_{t,D} = k_B T_{t,D}$ and total trap density of H_D at the donor HOMO band edge,

$$\begin{aligned} p_{It} &\approx H_D \exp\left(\frac{E_{HOMO,I} - E_{fp,I}}{k_B T_{t,D}}\right), \\ p_{It} &\approx H_D \left(\frac{p_I}{N_{HOMO}}\right)^{\frac{T}{T_{t,D}}}. \end{aligned} \tag{29}$$

Once the electron and hole densities are found at each position in the device, we use the definitions in Eq. (4) to find the electron quasi-Fermi level E_{fn},

$$E_{fn} = E_{LUMO} + k_B T ln(n/N_{LUMO}), \tag{30}$$

and the hole quasi-Fermi level E_{fp},

$$E_{fp} = E_{HOMO} - k_B T ln(p/N_{HOMO}). \tag{31}$$

The Shockley parameters in the SCD equation can then be evaluated using the expressions in Eqs. (10), (12), and (14)–(16). From

this construction, it is clear that if the equivalent circuit parameters are calculated in this way, the EEC provides a precise representation of the device model.

III. RESULTS

In this section, results for a typical bilayer OPV system are presented to illustrate the voltage dependence of the equivalent circuit parameters. Then, we apply our models to the dependence of these equivalent circuit parameters on donor hole mobility.

The devices studied are based on a P3HT/PCBM system that has the thicknesses of the donor and the acceptor layers of 50 nm and 22 nm.[45] Definitions and values of simulation parameters are summarized in Table I. The parameters result in a JV curve under illumination having $V_{oc} = 0.67$ V, $J_{sc} = -70\,\mathrm{Am}^{-2}$, and $FF = 67\%$, which are close to the values quoted in Ref. 45; i.e., $V_{oc} = 0.66$ V, $J_{sc} = -69Am^{-2}$, and $FF = 68\%$. We did not attempt a high resolution fit to the experimental data as we intend to use values typical of organic PVs not to fit a specific system. Unless stated otherwise, parameter values in Table I are used throughout this study as control variables.

TABLE I. Summary of definitions and values of important parameters used in simulations of P3HT/PCBM bilayer solar cells.

Parameter	Definition	Values
μ_p	Hole mobility in the donor and acceptor layers	2.0×10^{-8} m^2 V^{-1} s^{-1} 58
μ_n	Electron mobility in the donor and acceptor layers	2.0×10^{-7} m^2 V^{-1} s^{-1} 59
ϕ_a, ϕ_c	Injection barriers at the anode and the cathode $\phi_a = WF_{anode} - E_{HOMO,D}$ and $\phi_c = E_{LOMO,A} - WF_{anode}$, where WF denotes work function.	0.2 eV 60, 0.1 eV
ϵ	Dielectric permittivity of the donor and acceptor layers	$3.8\epsilon_0$ 61 and 62
$E_{t,A}$, $E_{t,D}$	Characteristic Urbach tail energies of exponential trapped electron and trapped hole distributions	$E_{t,A} = 40$ meV, $E_{t,D}$ 60 meV 62
$k_{PPr,0}$	The zero-field polaron pair recombination rate	$(30\,\mu s)^{-1}$
$E_{LUMO,D}$, $E_{HOMO,D}$	The LUMO and the HOMO energy levels of the donor	−3.0 eV, −4.9 eV 63 and 64
$E_{LUMO,A}$, $E_{HOMO,A}$	The LUMO and the HOMO energy levels of the acceptor	−3.7 eV, −6.1 eV 63 and 64
N_{HOMO}, N_{LUMO}	Densities of states at the HOMO and the LUMO band edges of both the donor and the acceptor	1.0×10^{27} m^{-3}
H_D, H_A	Total trap densities at the band edges of the donor and the acceptor	1.0×10^{24} m^{-3}
J_X	Exciton current density reaching the D–A interface	4.4×10^{20} m^{-2} s^{-1}
a_0	The D–A interface width	1.0 nm

In the following, we first show how the SCD Shockley parameters vary with applied voltage. Then, we vary donor hole mobility to illustrate how the voltage-dependent Shockley parameters change as the device physics changes. First, Fig. 3 presents the voltage dependence of dissociation and recombination quantities for the materials data in Table I. The figure shows that the approximation $k_{PPd}/k_{PPd,eq} \sim 1$, as used in Eq. (19), is a good approximation over most of the applied voltage range as the quantity R/R_{eq} is quite large over the voltage range considered.

A. Applied voltage dependence of SCD parameters

The way that the SCD Shockley parameters vary with the applied voltage at two intensities (1 sun and 0.1 suns), using the material's values of Table I, are presented in the bottom two panels of Fig. 4. These results are calculated from DD-BI device simulations using Eqs. (10), (12), (14), and (15) to find the Shockley parameters. Key quantities in these equations are presented in the top panel of the figure. Clearly, the SCD Shockley parameters are both voltage and intensity-dependent, and the origin of these behaviors is easy to trace to the device physics through the voltage dependences of the key device properties, as presented in the top panel of the figure.

In this particular case (see Table S4), the SCD Shockley parameters vary by an order of magnitude or more in going from the short-circuit to open-circuit conditions. The primary reason is the increase in charge density from the electrode injections, which reduces the series resistance. The increased carrier density also results in increased interface trapped carrier density, n_{It} and p_{It}, and changes the nature of trap-assisted recombination as indicated by the ideality factor, e.g., at one sun intensity, $n_{id} = 2.10$ at short circuit while at open circuit, it is 1.72. These changes cause the variations of the key quantities in Fig. 3, which directly affect the diode saturation current and parallel resistance. The strong dependence of the Shockley parameters on applied voltage leads to questions about the validity of extracting the correct physics insights

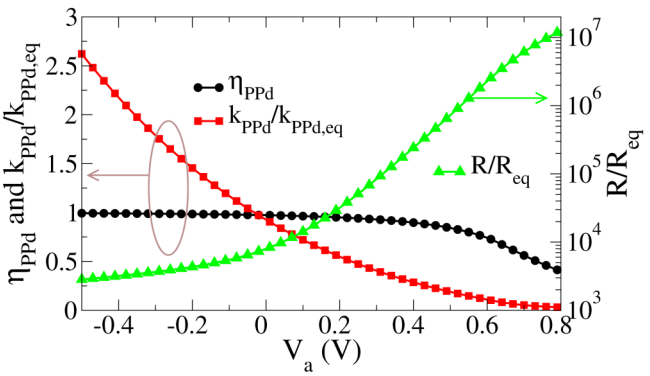

FIG. 3. Plots of η_{PPd}, $k_{PPd}/k_{PPd,eq}$, and R/R_{eq} as a function of V_a of a device with parameters in Table I.

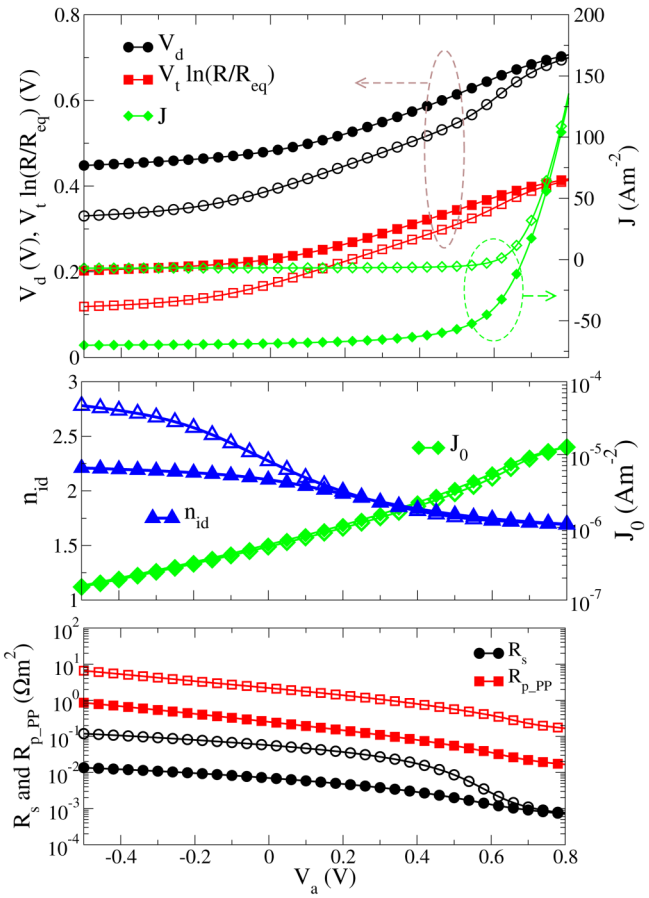

FIG. 4. Voltage dependences of key properties and the SCD Shockley parameters in the SCD model: (upper panel) V_d, $V_t ln(R/R_{eq})$, and J; (middle panel) n_{id} and J_0; and (bottom panel) R_s and R_{p_PP}, derived from DD-BI results under 1—sun intensity (opaque symbols) and 0.1—sun intensity (open symbols).

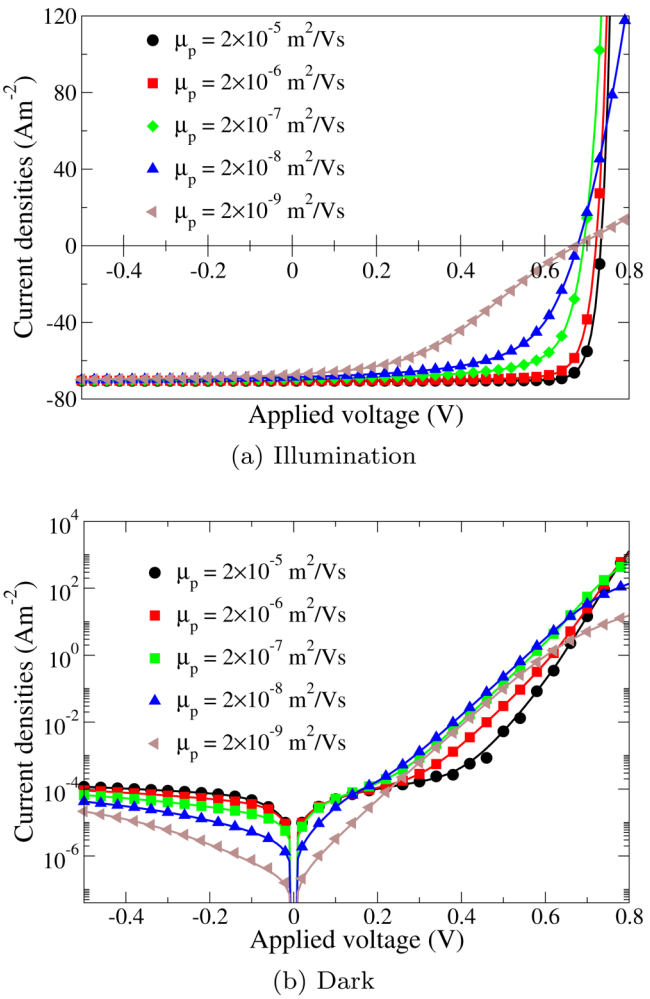

FIG. 5. Simulated JV curves under (a) illumination and (b) dark conditions of P3HT/PCBM bilayer devices with different hole mobilities.

when using constant Shockely parameters, as is typical in experimental studies of OPVs.[11]

B. Effects of changing the hole mobility

In many new OPV materials developing methods to increase the hole mobility is a challenge, and it is, thus, important to understand the effects of hole mobility on device physics. In this section, devices with hole mobilities (μ_p) in the range of 10^{-5} to 10^{-9} m^2/Vs are studied, and how the device physics changes the voltage dependence of the SCD Shockley parameter is discussed. The other materials values used in this section are taken from Table I.

Figure 5 shows JV curves calculated using the DD-BI (symbols) and the SCD (solid lines) models under illumination and dark conditions for the five different hole mobility values. Values of J_{sc}, V_{oc}, FF, and relative power conversion efficiency (PCE) of the devices under illumination are summarized in Table S5 and Fig. S5. Short-circuit current does not change noticeably as the hole mobilities reduce. The reduction of FF is the primary reason for losing PCE, and the trend agrees well with other works in the literature.[11,65,66] The s-shaped JV behavior is noticeable in the device with $\mu_p = 2 \times 10^{-9}$ $m^2V^{-1}s^{-1}$ because of charge accumulation in the active layer (see the discussion below)

Reductions of the dark current in the high V_a limit and the slopes around V_{oc} under illumination indicate an increment in R_s as a result of decreasing the hole mobility. Series resistance is usually related to carrier mobilities via the electrical conductivities,[11] $\sigma_n = q\mu_n n$ and $\sigma_p = q\mu_p p$, where n and p are free electron and hole densities, respectively. However, due to the fact that the charge densities are not constant in space [see Fig. 6(a)] because of space charge accumulation, the relationship between R_s and the electrical conductivity (or resistivity) has to be obtained via an

integral over the active layers' thicknesses. Here, we use the expression for R_s in terms of quasi-Fermi energies [see Eq. (12)], which is valid under any circumstances and fully treats space charge effects.

Figure 6 shows free hole density, free electron density (top figure), the quasi-Fermi energies, and band diagrams (bottom figure) as a function of position at short-circuit conditions ($V_a = 0$V). The density and potential profile are used to calculate energy level diagrams using Eq. (4) in Fig. 6(b). At thermal equilibrium, where $J_X = 0$ and $V_a = 0$, electron and hole density profiles decay exponentially from the electrodes and are almost invariant with changing μ_p. The reason for this behavior is that at equilibrium, the density of free carriers is small, so the applied coulomb potential from the electrodes is not screened. The LUMO and the HOMO bands then appear almost linear due to the linear potential dropped across the active layers, except near the electrodes where charges accumulate. Because total electron (J_n) and hole (J_p) currents have to be zero at equilibrium, i.e., $J_n(x) = \mu_n(x)n(x)\nabla E_{fn,eq}(x) = 0$ and $J_p(x) = \mu_p(x)p(x)\nabla E_{fp,eq}(x) = 0$,[31] equilibrium quasi-Fermi energies ($E_{fn,eq}$ and $E_{fp,eq}$) have to be spatially invariant and do not split from each other. Hence, based on these conditions and Eq. (4), n_{eq} and p_{eq} distribute exponentially from the electrodes to the D–A interface and are not affected by carrier mobilities.

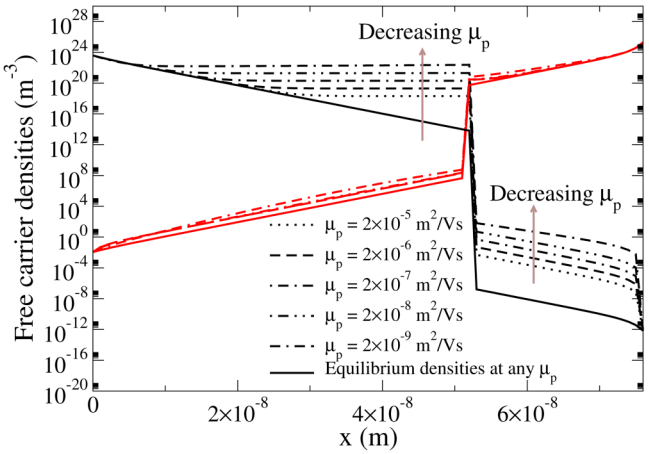

(a) Charge density profiles

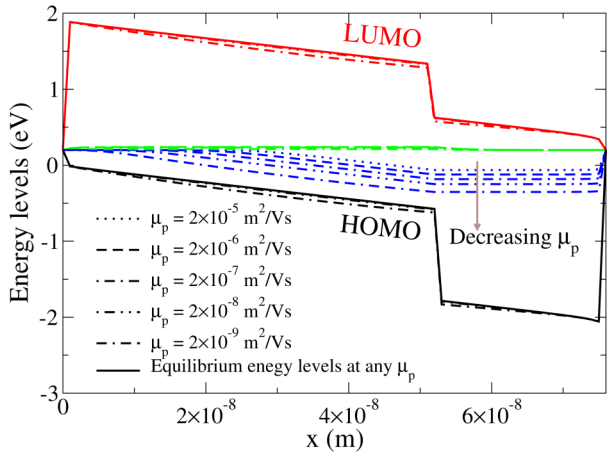

(b) Energy band diagrams

FIG. 6. Calculation results at short-circuit conditions ($V_a = 0$ V and $J_X = 4.4 \times 10^{22}$ m^{-2} s^{-1}) and at thermal equilibrium ($V_a = 0V$ and $J_X = 0$) of (a) hole densities (black lines) and electron densities (red lines) as a function of position—charge density profiles—of the devices with different μ_p values. (b) Energy band diagrams showing E_{fp} (blue lines), E_{fn} (green lines), HOMO (black lines), and LUMO (red lines) levels as a function of position calculated from the density profiles using Eq. (4).

Under illumination, photo-generation processes at the D–A interface produce a considerable number of carriers, resulting in higher majority charge densities around the D–A interface that screen the applied coulomb potential. Near the interface, the screened electric field leads to reduced drift currents and spatial invariance of majority interface charge accumulation. This process can be considered as space charge accumulation, and the degree of the accumulation depends on the mobilities, as shown in Fig. 6(a), i.e., there is more space charge accumulation when charge mobility is lower. In the device with $\mu_p = 2 \times 10^{-9}$ m^2 V^{-1} s^{-1}, the level of donor space charge accumulation is high, which significantly increases interface recombination and reduces charge extraction, giving rise to the s-shaped curve in Fig. 5. This high level of space charge accumulation is similar to the work by Wang *et al.*,[67] which introduces a thick exciton blocking layer to induce the s-shape effects.

According to Eq. (4), E_{fp} near the donor interface has to be parallel to E_{HOMO} because of the constant majority carrier density and *vice versa* for E_{fn} and E_{LUMO} in the acceptor. This process gives rise to a split of interface quasi-Fermi levels; $\Delta E_{fI} = E_{fn,I} - E_{fp,I}$, where $\Delta E_{fI}/q$ is the actual voltage driving the D–A interface—the diode voltage (V_d). Higher degrees of space charge accumulation from lower μ_p values bring E_{fp} closer to E_{HOMO}, resulting in the broader space charge region and a higher diode voltage.

C. Space charge effect on diode voltage

Diode voltages of the devices having different μ_p values from two different methods: (1) $qV_d = E_{fn,I} - E_{fp,I}$ and (2) $V_d = V_a - J(V_a)R_s$, where R_s is a constant from fitting, but $J(V_a)$ is from the simulations, are plotted in Fig. 7. Note that our V_d results agree with the internal voltage (V_{int}) in Ref. 11. The results indicate that a constant R_s cannot reproduce the actual diode voltage except in the voltage range near V_{oc} in high-mobility devices, which are not typical for OPVs. The lack of treatment of space charge effects near the interface when assuming a constant R_s causes the problems evident in this figure, while $qV_d = E_{fn,I} - E_{fp,I}$ already includes the space charge effects in the quasi-Fermi levels. The results here agree with those by Würfel *et al.*[11] with the following remarks.

First, for $V_a < V_{oc}$, V_d is always higher than V_a because of space charge accumulation near the D–A interface that splits the interface quasi-Fermi levels.[11] This accumulation of n_I and p_I causes an increase in Gibbs free energy density, $n_I E_{fn,I} - p_I E_{fp,I}$, in interface donor and acceptor molecules.[68] The change in the Gibbs free energy creates an electromotive force (*emf*), which is V_d in this case. The *emf* voltage must be larger than the external voltage (V_a)

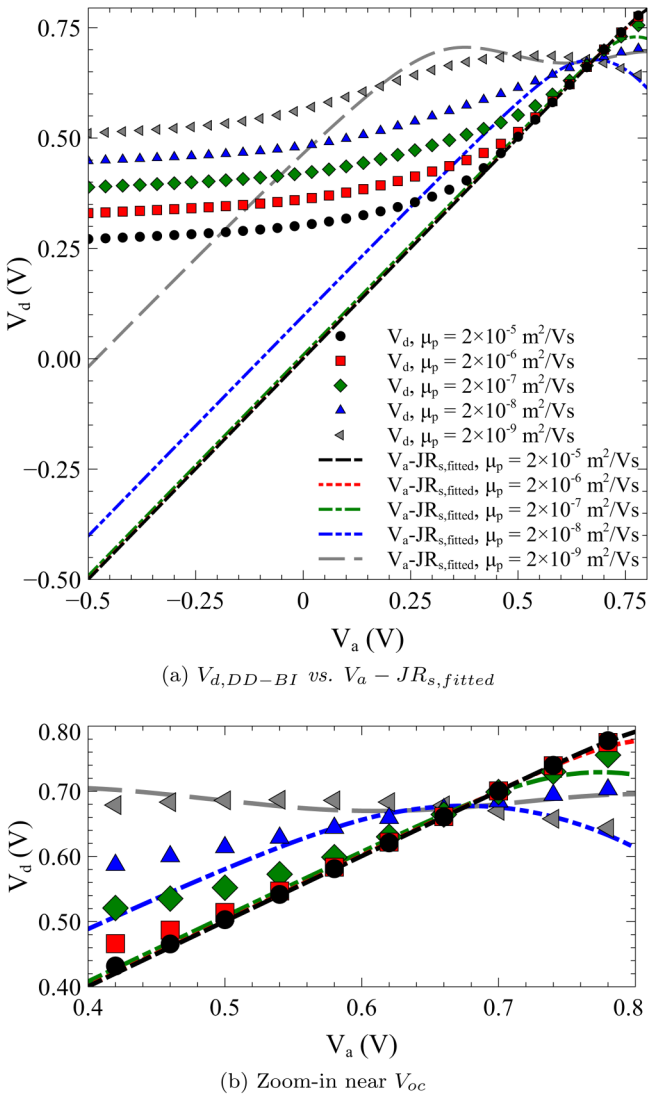

(a) $V_{d,DD-BI}$ *vs.* $V_a - JR_{s,fitted}$

(b) Zoom-in near V_{oc}

FIG. 7. Plots of (a) the diode voltages: $V_d = (E_{fn,I} - E_{fp,I})/q$, compared with V_d plots using the conventional equation: $V_d = V_a - JR_s$, where R_s is a constant fitting parameter and (b) a zoom-in area of the plot near open-circuit voltage.

during solar cell operation so that the internal voltage drives free carriers out of the cell. Using the expression $V_a - JR_s$, where R_s is a constant, results in an incorrect description of V_d, including prediction of negative values at low bias.

Second, the conventional relation $V_d = V_a - JR_s$, where R_s is a constant, found by fitting to experimental data describes V_d under illumination surprisingly well around V_{oc} [see Fig. 7(b)]. R_s around V_{oc} is relevant as the diode current that mainly depends on V_d becomes dominant there and determines the open-circuit JV slope and *FF*. $V_a - JR_s$ with constant R_s completely fails to predict V_d at low and reverse bias regimes, as these regimes are dominated by the voltage-dependent photocurrent ($-qJ_X\eta_{PPd}$). For these reasons, the Shockley equation with constant parameters usually fits experimental OPV JV curves under illumination. However, well-fitted parameters may not be able to provide physical insights because they do not include the voltage and illumination dependencies properly. Significant errors may arise in interpreting the physical meaning derived from using constant values of the fitting parameters.

D. Effects of carrier mobility on the voltage-dependent SCD parameters

Figure 8 shows the voltage-dependent SCD parameters in the devices having different μ_p values. It is known that carrier mobility

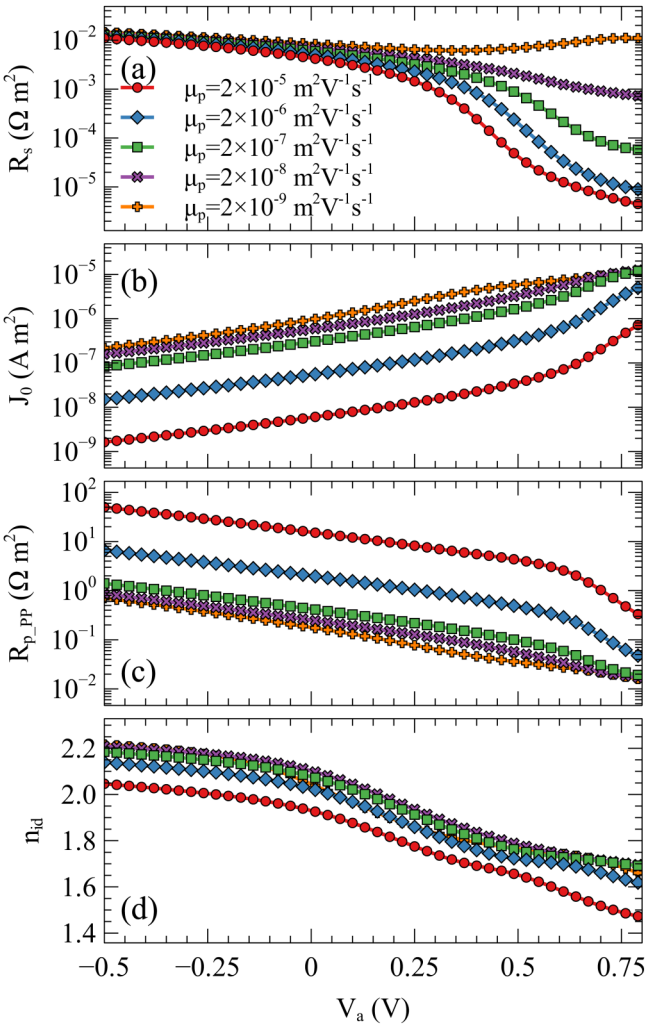

FIG. 8. The SCD parameters: (a) R_s, (b) J_0, (c) R_{p_PP}, and (d) n_{id}, as a function of V_a of the devices having different donor hole mobility values ranging from 2×10^{-9} m^2 V^{-1} s^{-1} to 2×10^{-5} m^2 V^{-1} s^{-1} calculated using Eqs. (10), (12), (14), and (15) with the DD-BI simulation results.

directly relates to the series resistance. However, carrier mobility also affects parallel resistance, diode saturation current, and the ideality factor due to space charge accumulation and recombination. Note that our R_s results are consistent with transport resistances measured using impedance spectroscopy by Guerrero *et al.*[12] The details about the voltage dependences of each SCD parameter are as follows.

According to the series resistance curves in the top panel of Fig. 8, R_s values of the devices having different μ_p values have greater difference at higher applied voltages than at the short-circuit conditions. At $V_a \approx 0$, the built-in potential extracts almost all the current J_X out of the cell as the photocurrent, making $\eta_{PPd} \approx 1$ and $J \approx -qJ_X$. This process is illustrated in Fig. 1 the rate J_X/a_0 on the left flowing through the PP states flows into the outgoing rate J/qa_0 on the right. In this situation, the densities ζ, n_I, and p_I are almost constant and balanced by the interface recombination and dissociation rates (see Fig. S6 in the supplementary material, for example). As a result, the interface electron–hole product ($n_I p_I$) is almost constant, as well as the split of quasi-Fermi levels because $E_{fn,I} - E_{fp,I} \propto k_B T \ln(n_I p_I)$ [see Eq. (4)]. These results explain the small variations of V_d trends in the negative and low V_a regimes in Fig. 7(a) and accordingly explain the convergence of the R_s functions in Fig. 8. At high voltages, devices having higher mobilities can be injected with carriers from the electrodes more easily as V_a increases, resulting in a higher degree of interface charge accumulation and quasi-Fermi level splitting. Hence, $\Delta E_{fI}/q$ of high-mobility devices will be closer to the external voltage, resulting in lower R_s values according to Eq. (12).

Moreover, in the high V_a limit, for injection barriers lower than 0.3 eV,[69] charge transport is dominated by injected charges from the electrodes. Space charge limited current (SCLC) limit[39,59,70,71] explains the current J following the relations $J \propto \mu V_a^2$ (i.e., Mott–Gurney law) or $J \propto \mu V_a^{m+1}$ if traps are present where $m = E_t/k_B T$ and E_t is the characteristic Urbach tail energy.[56,72] In this limit, R_s can be approximated by $[\partial J/\partial V_a]^{-1}$, so $R_s \propto \mu^{-1} V_a^{-m}$, which agrees with our results in Fig. 8, i.e., R_s at $V_a = 0.8V$ approximately varies with V_a^{-m}, where $m = 2.3$, and increases by about an order of magnitude when μ_p is lowered by an order of magnitude.

The second panel in Fig. 8 shows plots of J_0 of the devices. As described in Eq. (10), J_0 primarily depends on η_{PPd}, which varies from unity to zero as V_a increases. Plots of $\eta_{PPd}(V_a)$ functions are shown in Fig. S7 in the supplementary material. At high reverse bias, $\eta_{PPd} \to 1$ as PPs are efficiently dissociated by the built-in and applied voltages, so J_0 values are minimal due to the term $1 - \eta_{PPd}$. At the high V_a limit, $\eta_{PPd} \to 0$ as the applied voltage significantly suppresses PP dissociation. J_0 converges to $qa_0 R_{eq}$. Interestingly, R_{eq} is not significantly affected by the mobility, so J_0 functions with different μ_p values approximately converge to the same value at high V_a, as seen in the figure.

The third panel of Fig. 8 shows the R_{p_PP} functions of the devices having different μ_p values. JV curves with higher slopes at low V_a, for example, the device with $\mu_p = 2 \times 10^{-9}\ \mathrm{m^2\,V^{-1}\,s^{-1}}$, have higher magnitudes of the leakage current $qJ_X(1 - \eta_{PPd})$ and, thus, lower R_{p_PP} values. R_{p_PP} does not have a specific origin but it is associated with poor dissociation of PPs, i.e., η_{PPd}. Similarly to the conventional R_p, higher R_{p_PP} values are desirable.

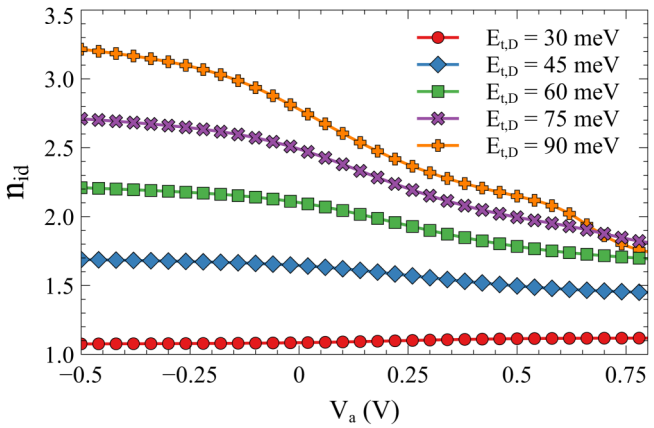

FIG. 9. Voltage-dependent ideality factor values calculated using Eq. (14) of the device with $\mu_p = 2 \times 10^{-8}\ \mathrm{m^2\,V^{-1}\,s^{-1}}$ but varying the width of donor tail states ($E_{t,D}$) from 30 to 90 meV.

To understand the n_{id} results in the bottom panel of Fig. 8, we first look into the correlations between n_{id} and trap characteristics. In Fig. 9, we plot voltage-dependent n_{id} values of the device with $\mu_p = 2 \times 10^{-8}\ \mathrm{m^2\,V^{-1}\,s^{-1}}$ but different characteristic widths of donor tail states ($E_{t,D}$) from 30 meV to 90 meV from the donor HOMO. The graphs confirm that deeper trap states result in higher n_{id} values. In devices with shallow traps, higher trapping and de-trapping rates between trap states and delocalized states result in interface trapped carrier densities (n_{It} and p_{It}) closer to free carrier densities (n_I and p_I). In this case, trap-assisted recombination in Eq. (27) will be similar to bimolecular recombination[53] and n_{id} approaches one. Moreover, the shift of recombination processes from trap-assisted recombination at low V_a to bimolecular recombination at higher V_a causes the voltage-dependent characteristics of n_{id}. Hence, we can understand from the n_{id} results in Fig. 8 that lower carrier mobility results in higher densities of trapped carriers and higher degrees of trap-assisted recombination.

E. Contributions of R_s, R_{p_PP}, and R_{p_local} to the measurement of resistance

We compare R_s, R_{p_PP}, and R_{p_local} with the total differential resistance, $R_{\mathrm{diff}} = [\partial J/\partial V_a]^{-1}$, of the device with $\mu_p = 2 \times 10^{-8}\ \mathrm{m^2\,V^{-1}\,s^{-1}}$ as a function of V_a in Fig. 10 in order to show that each resistance actually contributes to the measurable total cell resistance. In devices with non-ohmic JV behaviors, such as diodes and solar cells, the differential (or dynamic) resistance is often measured for analysis purposes.[73–75] Note that we use $R_{p\_local} = 2000\ \Omega\mathrm{m}^2$ for both under dark and illumination conditions, and note also that the leakage current $qJ_X(1 - \eta_{PPd})$ is zero in the dark, so R_{p_PP} is infinitely high (i.e., does not play a role).

Under illumination, at low and negative V_a, the diode current is irrelevant as recombination of free carriers is very low, so recombination current is conducted by J_{leak} and $qJ_X(1 - \eta_{PPd})$. The two leakage currents are under the same bias of V_d, but $R_{p\_local} \gg R_{p\_PP}$, so total leakage current in this regime is

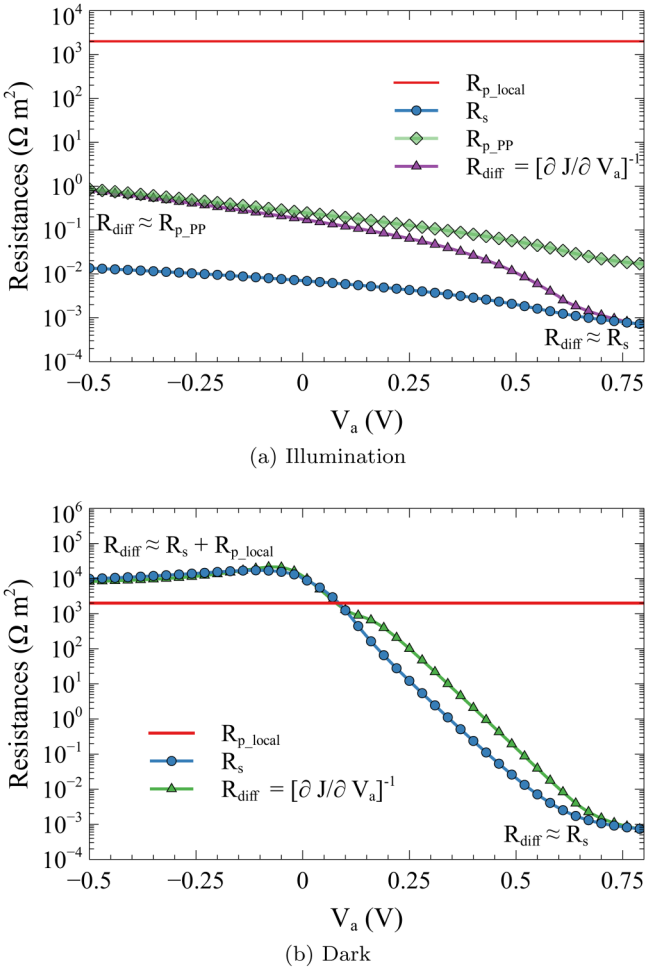

FIG. 10. Plots of R_s, R_{p_PP}, and R_{p_local} as a function of applied voltage compared to the total differential resistance ($R_{diff} = [\partial J/\partial V_a]^{-1}$) of the device with $\mu_p = 2 \times 10^{-8}\ m^2\ V^{-1}\ s^{-1}$ under (a) illumination and (b) dark conditions. Note that constant $R_{p\_local} = 2000\ \Omega m^2$ is used in both cases.

dominated by $qJ_X(1 - \eta_{PPd})$, and thus only R_{p_PP} contributes to the total device resistance [see Eq. (17)]. This prediction excellently agrees with R_{diff} in Fig. 10(a). As V_a increases, the diode current increases, resulting in reducing R_{diff} values. Once the diode current dominates, R_s, which primarily governs the diode term through the diode voltage, becomes the dominant resistance, and $R_{diff} \rightarrow R_s$, which is clearly exhibited in the plot.

In the dark, only R_s and R_{p_local} contribute to the total resistance. At negative V_a where the diode current is negligible, R_s and R_{p_local} are connected in series (see Fig. 2 for an illustration). Consequently, $R_{diff} \approx R_s + R_{p\_local}$, which agrees with Fig. 10(b). At low positive V_a, R_s reduces from the higher numbers of injected carriers. However, both R_s and R_{p_local} still play a role and result in R_{diff} being an interpolation between the two resistances. Above a threshold voltage that activates the diode, the majority of the total dark current is the diode current, so R_s dominates the resistances and $R_{diff} \rightarrow R_s$.

As we can see from the results, R_s, R_{p_PP}, and R_{p_local} are associated with well defined physical properties and contribute in different ways to the measured differential resistance. This result is another example of the validity and utility of the SCD equation in describing the correct physics of OPVs.

IV. CONCLUSIONS

We presented the SCD equation, which is equivalent to the Shockley equation but with voltage-dependent parameters, based on the DD-BI device model that solves the charge transport equations self-consistently. The two models provide physical definitions of Shockley parameters that are self-consistent and physically meaningful.

First, the diode saturation current, which is given by $J_0 = qa_0(1 - \eta_{PPd})R_{eq}$, is a modified equilibrium recombination current under bias. It can vary many orders of magnitude under bias as it depends on the term $1 - \eta_{PPd}$ but it can roughly predict the equilibrium recombination rate as $J_0 \approx qa_0R_{eq}$ in the high V_a limit.

For R_s, the relation $V_d = V_a - JR_s = \Delta E_{fl}/q$, where V_a is the difference between the electrode Fermi energies in electronvolt under bias, defines R_s as a resistance that spatially changes E_{fn} and E_{fp}, in eV, from the electrodes to the D–A interface. At solar cell operation voltages, $\Delta E_{fl}/q$ is higher than V_a, so there is an electromotive force driving photo-generated charges to the external circuit. A constant fitted R_s cannot reproduce the nature of V_d because space charge effects are not included. Constant R_s can only result in reasonable $\Delta E_{fl}/q$ values around V_{oc} in high-mobility devices and should be used for comparison purposes.

For R_p, we find that two sources of R_p with very different values are needed to simulate a device both under illumination and dark conditions correctly. The first one is R_{p_local} from actual leakage pathways, such as pinholes. The other is the recombination resistance R_{p_PP} from overall recombined PPs that causes a virtual leakage current of $qJ_X(1 - \eta_{PPd})$. Total parallel resistance is $R_p = (1/R_{p\_local} + 1/R_{p\_PP})^{-1}$, where only R_{p_local} dominates in the dark and only R_{p_PP} typically dominates under illumination.

An ideality factor measures the change of free carrier recombination rate relative to the equilibrium value under the influence of the diode voltage, $n_{id} = \Delta E_{fl}/V_t ln(R/R_{eq})$. We show that this form of n_{id} yields valid n_{id} values that correlate to the trap characteristics and recombination processes.

This paper points out the importance of the voltage dependence of Shockley diode equation parameters for a complete description of OPV device physics when space charge effects are important. Though obtaining the true voltage-dependent functions is challenging experimentally, a combined experimental/device model approach is likely to be productive in many cases using the methodology presented here. Though the analysis here concentrates on the DD-BI model using the GWWF model, the voltage dependence of the associated Shockley parameters is expected to be robust for devices where space charge effects are important, as demonstrated in the supplementary material for the case of SRH recombination kinetics. Key to the analysis described here are the

explicit relations between DD-BI results and Shockley equation parameters. It is important to extend this work to include additional physical processes to enable fully quantitative extraction of voltage dependent parameters for a wide range of OPV devices.

SUPPLEMENTARY MATERIAL

See the supplementary material for the details of implementing the DD-BI model, the validity conditions of the reduce form of the SRH recombination via tail states, values of the SCD parameters: R_{p_PP}, R_s, J_0, and n_{id}, at short-circuit and open-circuit conditions under 0.1—sun and 1—sun illumination intensities, efficiency parameters, interface densities, and polaron pair dissociation probability of the devices with different hole mobility values.

ACKNOWLEDGMENTS

This research project is supported by Thailand Science Research and Innovation (TSRI) Basic Research Fund: Fiscal year 2021 under Project No. 64A306000005. Early work of this study was a part of Dr. Non Thongprong's Ph.D. thesis research at Michigan State University (MSU) and was supported by the Thai government through the Development and Promotion of Science and Technology Talents Project (DPST) scholarship and by the Physics and Astronomy Department at MSU.

DATA AVAILABILITY

The data that support the findings of this study are available from the corresponding authors upon reasonable request.

REFERENCES

[1]W. Shockley, "The theory of p-n junctions in semiconductors and p-n junction transistors," Bell Labs Tech. J. **28**, 435–489 (1949).
[2]J. D. Servaites, S. Yeganeh, T. J. Marks, and M. A. Ratner, "Efficiency enhancement in organic photovoltaic cells: Consequences of optimizing series resistance," Adv. Funct. Mater. **20**, 97–104 (2010).
[3]B. P. Rand, D. P. Burk, and S. R. Forrest, "Offset energies at organic semiconductor heterojunctions and their influence on the open-circuit voltage of thin-film solar cells," Phys. Rev. B **75**, 115327 (2007).
[4]D. Cheyns, J. Poortmans, P. Heremans, C. Deibel, S. Verlaak, B. Rand, and J. Genoe, "Analytical model for the open-circuit voltage and its associated resistance in organic planar heterojunction solar cells," Phys. Rev. B **77**, 165332 (2008).
[5]A. Foertig, J. Rauh, V. Dyakonov, and C. Deibel, "Shockley equation parameters of P3HT: PCBM solar cells determined by transient techniques," Phys. Rev. B **86**, 115302 (2012).
[6]B. Qi and J. Wang, "Fill factor in organic solar cells," Phys. Chem. Chem. Phys. **15**, 8972–8982 (2013).
[7]J. D. Servaites, M. A. Ratner, and T. J. Marks, "Organic solar cells: A new look at traditional models," Energy Environ. Sci. **4**, 4410–4422 (2011).
[8]H. Hoppe and N. S. Sariciftci, "Organic solar cells: An overview," J. Mater. Res. **19**, 1924–1945 (2004).
[9]C. Deibel, A. Wagenpfahl, and V. Dyakonov, "Influence of charge carrier mobility on the performance of organic solar cells," Phys. Status Solidi Rapid Res. Lett. **2**, 175–177 (2008).
[10]C. Deibel, T. Strobel, and V. Dyakonov, "Role of the charge transfer state in organic donor–acceptor solar cells," Adv. Mater. **22**, 4097–4111 (2010).
[11]U. Würfel, D. Neher, A. Spies, and S. Albrecht, "Impact of charge transport on current–voltage characteristics and power-conversion efficiency of organic solar cells," Nat. Commun. **6**, 1–9 (2015).
[12]A. Guerrero, T. Ripolles-Sanchis, P. P. Boix, and G. Garcia-Belmonte, "Series resistance in organic bulk-heterojunction solar devices: Modulating carrier transport with fullerene electron traps," Org. Electron. **13**, 2326–2332 (2012).
[13]T. Kuwabara, Y. Kawahara, T. Yamaguchi, and K. Takahashi, "Characterization of inverted-type organic solar cells with a ZnO layer as the electron collection electrode by ac impedance spectroscopy," ACS Appl. Mater. Interfaces **1**, 2107–2110 (2009).
[14]M. Turek, "Current and illumination dependent series resistance of solar cells," J. Appl. Phys. **115**, 144503 (2014).
[15]N. C. Giebink, G. P. Wiederrecht, M. R. Wasielewski, and S. R. Forrest, "Ideal diode equation for organic heterojunctions. I. Derivation and application," Phys. Rev. B **82**, 155305 (2010).
[16]D. Liraz, H. Shekhar, L. Tzabari, and N. Tessler, "Benchmarking the electronic processes at the planar organic heterojunction solar cells," J. Phys. Chem. C **122**, 23271–23279 (2018).
[17]L. J. Koster, E. Smits, V. Mihailetchi, and P. Blom, "Device model for the operation of polymer/fullerene bulk heterojunction solar cells," Phys. Rev. B **72**, 085205 (2005).
[18]G. A. Buxton and N. Clarke, "Computer simulation of polymer solar cells," Model. Simul. Mater. Sci. Eng. **15**, 13 (2006).
[19]B. Y. Finck and B. J. Schwartz, "Understanding the origin of the s-curve in conjugated polymer/fullerene photovoltaics from drift-diffusion simulations," Appl. Phys. Lett. **103**, 053306 (2013).
[20]J. A. Barker, C. M. Ramsdale, and N. C. Greenham, "Modeling the current-voltage characteristics of bilayer polymer photovoltaic devices," Phys. Rev. B **67**, 075205 (2003).
[21]Y. Zhang, X. Li, T. Dai, W. Ha, H. Du, S. Li, K. Wang, F. Meng, D. Xu, and A. Geng, "Charge transport and extraction of bilayer interdiffusion heterojunction organic solar cells," J. Phys. Chem. C **123**, 24446–24452 (2019).
[22]C. J. Traverse, M. Young, J. Suddard-Bangsund, T. Patrick, M. Bates, P. Chen, B. Wingate, S. Y. Lunt, A. Anctil, and R. R. Lunt, "Anions for near-infrared selective organic salt photovoltaics," Sci. Rep. **7**, 1–8 (2017).
[23]M. Bates and R. R. Lunt, "Organic salt photovoltaics," Sustainable Energy Fuels **1**, 955–968 (2017).
[24]N. D. Treat, M. A. Brady, G. Smith, M. F. Toney, E. J. Kramer, C. J. Hawker, and M. L. Chabinyc, "Interdiffusion of PCBM and P3HT reveals miscibility in a photovoltaically active blend," Adv. Energy Mater. **1**, 82–89 (2011).
[25]F. Liu, Y. Gu, J. W. Jung, W. H. Jo, and T. P. Russell, "On the morphology of polymer-based photovoltaics," J. Polym. Sci. B **50**, 1018–1044 (2012).
[26]D. Veldman, S. C. Meskers, and R. A. Janssen, "The energy of charge-transfer states in electron donor–acceptor blends: Insight into the energy losses in organic solar cells," Adv. Funct. Mater. **19**, 1939–1948 (2009).
[27]J.-L. Brédas, J. E. Norton, J. Cornil, and V. Coropceanu, "Molecular understanding of organic solar cells: The challenges," Acc. Chem. Res. **42**, 1691–1699 (2009).
[28]T. M. Clarke and J. R. Durrant, "Charge photogeneration in organic solar cells," Chem. Rev. **110**, 6736–6767 (2010).
[29]C. L. Braun, "Electric field assisted dissociation of charge transfer states as a mechanism of photocarrier production," J. Chem. Phys. **80**, 4157–4161 (1984).
[30]V. Mihailetchi, L. Koster, J. Hummelen, and P. Blom, "Photocurrent generation in polymer-fullerene bulk heterojunctions," Phys. Rev. Lett. **93**, 216601 (2004).
[31]J. Nelson, *The Physics of Solar Cells* (World Scientific Publishing Co Inc, 2003).
[32]T. Kirchartz, F. Deledalle, P. S. Tuladhar, J. R. Durrant, and J. Nelson, "On the differences between dark and light ideality factor in polymer: Fullerene solar cells," J. Phys. Chem. Lett. **4**, 2371–2376 (2013).
[33]G. Lakhwani, A. Rao, and R. H. Friend, "Bimolecular recombination in organic photovoltaics," Annu. Rev. Phys. Chem. **65**, 557–581 (2014).
[34]C. Groves and N. Greenham, "Bimolecular recombination in polymer electronic devices," Phys. Rev. B **78**, 155205 (2008).
[35]R. Street, K. Song, and S. Cowan, "Influence of series resistance on the photocurrent analysis of organic solar cells," Org. Electron. **12**, 244–248 (2011).

[36]Y. Shen, K. Li, N. Majumdar, J. C. Campbell, and M. C. Gupta, "Bulk and contact resistance in P3HT: PCBM heterojunction solar cells," Solar Energy Mater. Solar Cells **95**, 2314–2317 (2011).
[37]B. Qi and J. Wang, "Open-circuit voltage in organic solar cells," J. Mater. Chem. **22**, 24315–24325 (2012).
[38]D. Credgington and J. R. Durrant, "Insights from transient optoelectronic analyses on the open-circuit voltage of organic solar cells," J. Phys. Chem. Lett. **3**, 1465–1478 (2012).
[39]A. Moliton and J.-M. Nunzi, "How to model the behaviour of organic photovoltaic cells," Polym. Int. **55**, 583–600 (2006).
[40]V. S. Balderrama, J. Albero, P. Granero, J. Ferré-Borrull, J. Pallarés, E. Palomares, and L. F. Marsal, "Design, fabrication and charge recombination analysis of an interdigitated heterojunction nanomorphology in P3HT/$PC_{70}BM$ solar cells," Nanoscale **7**, 13848–13859 (2015).
[41]G. Hurkx, D. Klaassen, and M. Knuvers, "A new recombination model for device simulation including tunneling," IEEE Trans. Electron Devices **39**, 331–338 (1992).
[42]C. Yoo and T. W. Kim, "Tunneling processes and leakage current mechanisms of thin organic layer sandwiched between two electrodes," Curr. Appl. Phys. **16**, 170–174 (2016).
[43]C. K. Renshaw, J. D. Zimmerman, B. E. Lassiter, and S. R. Forrest, "Photoconductivity in donor-acceptor heterojunction organic photovoltaics," Phys. Rev. B **86**, 085324 (2012).
[44]W.-I. Jeong, Y. E. Lee, H.-S. Shim, T.-M. Kim, S.-Y. Kim, and J.-J. Kim, "Photoconductivity of C60 as an origin of bias-dependent photocurrent in organic photovoltaics," Adv. Funct. Mater. **22**, 3089–3094 (2012).
[45]A. L. Ayzner, C. J. Tassone, S. H. Tolbert, and B. J. Schwartz, "Reappraising the need for bulk heterojunctions in polymer-fullerene photovoltaics: The role of carrier transport in all-solution-processed P3HT/PCBM bilayer solar cells," J. Phys. Chem. C **113**, 20050–20060 (2009).
[46]J. R. Tumbleston, D.-H. Ko, E. T. Samulski, and R. Lopez, "Nonideal parasitic resistance effects in bulk heterojunction organic solar cells," J. Appl. Phys. **108**, 084514 (2010).
[47]L. Li, N. Lu, M. Liu, and H. Bässler, "General Einstein relation model in disordered organic semiconductors under quasiequilibrium," Phys. Rev. B **90**, 214107 (2014).
[48]O. Magen and N. Tessler, "On electrode pinning and charge blocking layers in organic solar cells," J. Appl. Phys. **121**, 195502 (2017).
[49]H. K. Gummel, "A self-consistent iterative scheme for one-dimensional steady state transistor calculations," IEEE Trans. Electron Devices **11**, 455–465 (1964).
[50]N. C. Giebink, B. E. Lassiter, G. P. Wiederrecht, M. R. Wasielewski, and S. R. Forrest, "Ideal diode equation for organic heterojunctions. II. The role of polaron pair recombination," Phys. Rev. B **82**(15), 155306 (2010).
[51]W. Shockley and W. Read Jr., "Statistics of the recombinations of holes and electrons," Phys. Rev. **87**, 835 (1952).
[52]R. N. Hall, "Electron-hole recombination in germanium," Phys. Rev. **87**, 387 (1952).
[53]M. Kuik, L. Koster, G. Wetzelaer, and P. Blom, "Trap-assisted recombination in disordered organic semiconductors," Phys. Rev. Lett. **107**, 256805 (2011).
[54]T. Kirchartz, B. E. Pieters, J. Kirkpatrick, U. Rau, and J. Nelson, "Recombination via tail states in polythiophene: Fullerene solar cells," Phys. Rev. B **83**, 115209 (2011).
[55]S. A. Hawks, G. Li, Y. Yang, and R. A. Street, "Band tail recombination in polymer: Fullerene organic solar cells," J. Appl. Phys. **116**, 074503 (2014).
[56]P. Mark and W. Helfrich, "Space-charge-limited currents in organic crystals," J. Appl. Phys. **33**, 205–215 (1962).
[57]N. Tessler, Y. Preezant, N. Rappaport, and Y. Roichman, "Charge transport in disordered organic materials and its relevance to thin-film devices: A tutorial review," Adv. Mater. **21**, 2741–2761 (2009).
[58]R. Mauer, M. Kastler, and F. Laquai, "The impact of polymer regioregularity on charge transport and efficiency of P3HT: PCBM photovoltaic devices," Adv. Funct. Mater. **20**, 2085–2092 (2010).
[59]V. D. Mihailetchi, J. K. van Duren, P. W. Blom, J. C. Hummelen, R. A. Janssen, J. M. Kroon, M. T. Rispens, W. J. H. Verhees, and M. M. Wienk, "Electron transport in a methanofullerene," Adv. Funct. Mater. **13**, 43–46 (2003).
[60]F. Zhang, A. Vollmer, J. Zhang, Z. Xu, J. Rabe, and N. Koch, "Energy level alignment and morphology of interfaces between molecular and polymeric organic semiconductors," Org. Electron. **8**, 606–614 (2007).
[61]C. Shuttle, R. Hamilton, B. O'Regan, J. A. Nelson, and J. Durrant, "Charge-density-based analysis of the current–voltage response of polythiophene/fullerene photovoltaic devices," Proc. Natl. Acad. Sci. U.S.A. **107**, 16448–16452 (2010).
[62]R. C. MacKenzie, C. G. Shuttle, M. L. Chabinyc, and J. Nelson, "Extracting microscopic device parameters from transient photocurrent measurements of P3HT: PCBM solar cells," Adv. Energy Mater. **2**, 662–669 (2012).
[63]H. Kim, M. Shin, and Y. Kim, "Influence of thermal annealing on the deformation of a lithium fluoride nanolayer in polymer: Fullerene solar cells," Europhys. Lett. **84**, 58002 (2008).
[64]B. Ray and M. A. Alam, "Random vs regularized OPV: Limits of performance gain of organic bulk heterojunction solar cells by morphology engineering," Sol. Energy Mater. Sol. Cells **99**, 204–212 (2012).
[65]W. Tress, A. Petrich, M. Hummert, M. Hein, K. Leo, and M. Riede, "Imbalanced mobilities causing s-shaped IV curves in planar heterojunction organic solar cells," Appl. Phys. Lett. **98**, 23 (2011).
[66]B. Xiao, M. Zhang, J. Yan, G. Luo, K. Gao, J. Liu, Q. You, H.-B. Wang, C. Gao, B. Zhao *et al.*, "High efficiency organic solar cells based on amorphous electron-donating polymer and modified fullerene acceptor," Nano Energy **39**, 478–488 (2017).
[67]J. Wang, X. Ren, S. Shi, C. Leung, and P. K. Chan, "Charge accumulation induced S-shape J–V curves in bilayer heterojunction organic solar cells," Org. Electron. **12**, 880–885 (2011).
[68]J. Parrott, "Thermodynamics of solar cell efficiency," Sol. Energy Mater. Sol. Cells **25**, 73–85 (1992).
[69]A. Kokil, K. Yang, and J. Kumar, "Techniques for characterization of charge carrier mobility in organic semiconductors," J. Polym. Sci. B **50**, 1130–1144 (2012).
[70]V. Mihailetchi, J. Wildeman, and P. Blom, "Space-charge limited photocurrent," Phys. Rev. Lett. **94**, 126602 (2005).
[71]P. L. Varo, J. J. Tejada, J. L. Villanueva, J. Carceller, and M. Deen, "Modeling the transition from ohmic to space charge limited current in organic semiconductors," Org. Electron. **13**, 1700–1709 (2012).
[72]J. Dacuña and A. Salleo, "Modeling space-charge-limited currents in organic semiconductors: Extracting trap density and mobility," Phys. Rev. B **84**, 195209 (2011).
[73]M. Bashahu and A. Habyarimana, "Review and test of methods for determination of the solar cell series resistance," Renew. Energy **6**, 129–138 (1995).
[74]J. Halme, P. Vahermaa, K. Miettunen, and P. Lund, "Device physics of dye solar cells," Adv. Mater. **22**, E210 (2010).
[75]W. L. Leong, S. R. Cowan, and A. J. Heeger, "Differential resistance analysis of charge carrier losses in organic bulk heterojunction solar cells: Observing the transition from bimolecular to trap-assisted recombination and quantifying the order of recombination," Adv. Energy Mater. **1**, 517–522 (2011).